**“Alexandru Ioan Cuza” University of Iasi**
**Faculty of Physics**

Abstract of the PhD thesis

# STUDY OF THIN FILMS AND MULTILAYER STRUCTURES USED FOR FUNCTIONAL APPLICATIONS

**Scientific adviser,**
**Prof. Dr. Felicia Iacomi**

**PhD student,**
**Gheorghe ZODIERIU**

**- Iaşi 2013 -**

**“Alexandru Ioan Cuza” University of Iasi**
**In attention of**
**.....**

We inform you that on June 28, 2013, 11:00 a.m., in room L1, Mr. Gheorghe Zodieriu will present the PhD thesis ***Study of thin films and multilayer structures used for functional applications***, in public meeting, in order to obtain the Doctor in Physics scientific title.

Doctoral committee has the following members:

| | |
|---|---|
| Prof dr. Diana - Mihaela MARDARE | *Chairman*<br>Director of the Doctoral School<br>Faculty of Physics<br>“Al. I. Cuza” University of Iasi |
| Prof. dr. Felicia IACOMI | *Scientific adviser*<br>Faculty of Physics<br>“Al. I. Cuza” University of Iasi |
| Conf. dr. Liviu Leontie | *Reviewer*<br>Faculty of Physics<br>“Al. I. Cuza” University of Iasi |
| C.S.I dr. Munizer PURICA | *Reviewer*<br>National Institute for Research and Development in Microtechnologies - IMT Bucharest |
| C.S.II dr. Daniel TÎMPU | *Reviewer*<br>„Petru Poni” Institute of Macromolecular Chemistry, Iaşi |

We invite you to attend at the public meeting to present the thesis.

## Content

# INTRODUCTION

This thesis aims to make contributions in thin films and multilayer structures domain, with applications in optoelectronics, spintronics and sensors.

The work is divided into four chapters. The first chapter is an overview of the main trends in the functional thin layers field. The second chapter summarizes the main methods of obtaining and characterization of the thin films and multilayer structures. In the third chapter are presented the original contributions regarding multi-layer structures based on oxides like TiO2 and SiO2. The experimental results led to achieve a bandpass filter in visible. In the fourth chapter the results on the three classes of materials are presented.

Significant results were obtained regarding the effect of the deposition method on the structure and chemical composition of thin films and magnetic and as sensor properties were revealed, recommending the analyzed thin layers in spintronics and in sensors applications.

We concluded that the full understanding of the growth and deposition processes is the cornerstone for applications in microelectronic and sensor devices.

# CHAPTER III
# THIN FILMS AND MULTILAYER STRUCTURES WITH SELECTIVE SPECTRAL PROPERTIES

## 3.1. Introduction

Multilayer systems which are operating based on optical interference are formed from structures of thin films consisting layers with different refractive indices. Transparent oxide layers are used as highly reflective or antireflective coatings,

band pass filters, narrowband filters in various optical and electronic devices [1-12].

$TiO_2$ is one of the most interesting dielectric materials because it is transparent in the visible light region, has a high refractive index, low absorption, good hardness and forms with $SiO_2$, in discrete or mixed coatings, stable devices [14,15]. $SiO_2$ is a low refractive index material, is transparent from UV to near IR [16].

$TiO_2$ – $SiO_2$ systems are extensively used in making a wide varieties of optical devices. Oullette et al. reported the ability to prepare a $TiO_2$ – $SiO_2$ stop band filter by reactive sputter deposition [4]. Wong et al. reported the preparation of a reflective optical filter using mixed $TiO_2$ and $SiO_2$ multilayer, achieving different values of refractive index (n = 1.47 – 2.2) [18].

## 3.2. Technological experiments for thin films and multilayer structures deposition

### 3.2.1 Technological experiments for metal layers deposition

In this study we selected metal materials and oxide materials suitable for making multi-layer structures with selective spectral properties. For this purpose, some improvements have been brought to the VUP-5M deposition installation by designing the rotating system of the samples and masks, and by adaptation the heating system of the substrate, in order to achieve rotation and simultaneous heating of the substrates.

To successive deposition of the multilayer structures a model has been designed, to achieve a rotation system of the samples from a target to another and the corresponding change of masks (Figure 3.7).

Since the installation allows substrate heating without being rotated, a device allowing the substrate rotation and heating, to

obtain uniform and good quality thin films, has been realized (Fig.3.8).

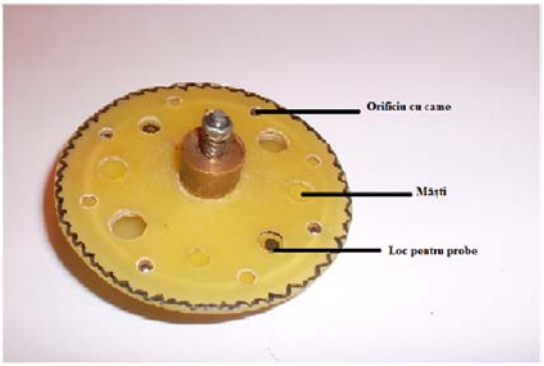


Fig.3.7. Samples and masks rotation system for the thin layers successive deposition

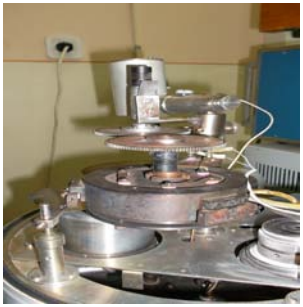

Fig.3.8. Heating and rotating system of the sample holder

## 3.3. Structural and functional characterization of thin films and multilayer structures

### 3.3.1. Study the structure and morphology of the metal oxide thin films

Thin films and multilayer structures have been subjected to a structural characterization using x-ray diffraction (DRON 2, $CuK_{\alpha}$). The morphology and surface roughness was analyzed by atomic force microscopy using a NT - MDT Solver Pro 7M platform and by scanning electron microscopy using an equipped with a device for determination of the elemental chemical composition, VEGA II LSH EDX - QUANTAX QX2.

We have investigated the conditions for the deposition of the metal layers and also their nature, to obtain semi-transparent conducting electrodes. It has been shown that thin layers of Al obtained by thermal evaporation in vacuum, with

deposition time of 20 seconds and Ag thin films obtained at the deposit time of 16 seconds are optimal for such applications.

XRD patterns of the thin films of titanium oxide, silicon oxide, or thin layers of metal (Al, Ag) deposited on glass substrate maintained at room temperature, highlight their amorphous nature.

The same system $Ag/TiO_2/SiO_2/TiO_2/SiO_2/Ag$ deposited under the same conditions, but on textile substrate, shows a XRD pattern expressing the nanocrystalline nature of the structure (Fig. 3.15). The XRD peaks belonging to anatase phase of the titanium oxide and the XRD peaks belonging to α-quartz crystalline phase of the silicon oxide were highlighted. Intense peaks are due to the greater thickness of the layer of silicon oxide relative to titanium oxide.

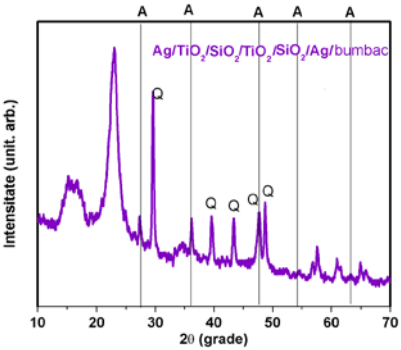


Fig.3.15**.** XRD pattern for the multilayer system obtained according to the technological flow presented in Fig. 3.9. (Ti target, D = 4 cm, the substrate is at room temperature), A - $TiO_2$ anatase phase;. Q - α-quartz

### 3.3.1.2. Investigation of the thin films morphology and surface roughness

From the analysis of the $3x3\mu m^2$ and $1x1\mu m^2$ 2D and 3D AFM images (Fig.3.16 - Fig.3.23) the nanostructured character of

the thin metal layers is observed, the roughness being of the 1.5 nm orders.

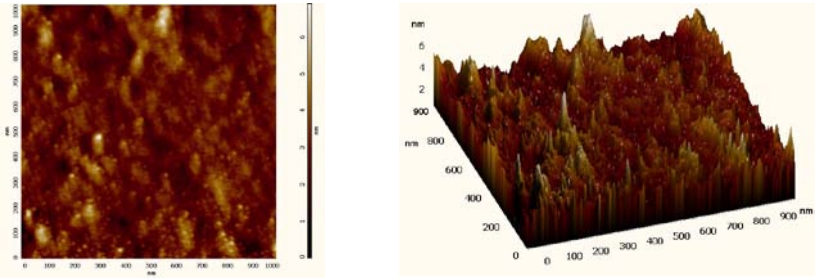

Fig.3.20**.** 2D and 3D images of $TiO_2$ thin film deposited by spray reactive dc magnetron, Ti target, I = 100mA, $Ar/O_2$=1,21; D=4cm, t=1h, T=20 $^0$C, RMS=0.11 nm

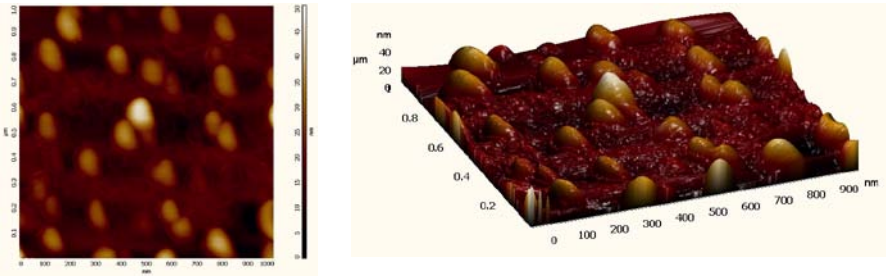

Fig.3.21. 2D and 3D images of $TiO_2$ thin film deposited by spray reactive dc magnetron, Ti target, I = 100mA, $Ar/O_2$=1,21 D=4cm, t=1h, T =500$^o$C, RMS =4.73 nm

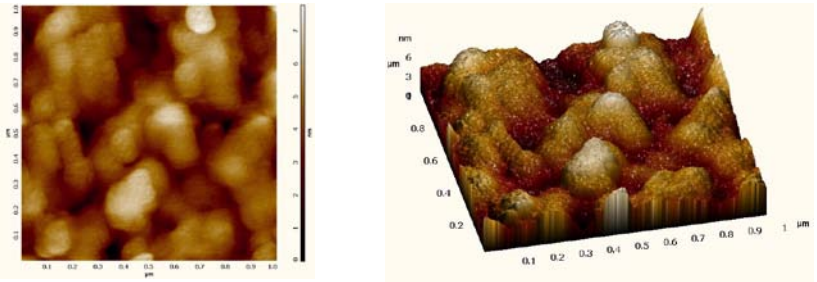

Fig.3.22. 2D and 3D images of thin SiO2 layer deposited by reactive rf magnetron sputtering, Si target, P =50W, $Ar/O_2$=1,21 D = 4cm, t = 1h, RMS=0,91 nm.

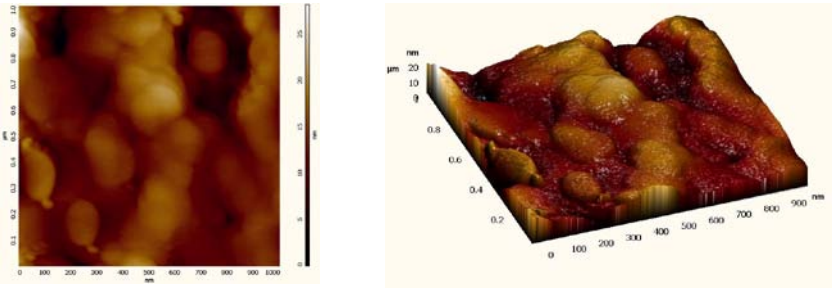

Fig.3.23. 2D and 3D images of thin SiO2 layer deposited by reactive rf magnetron sputtering, Si target, P =50W, $Ar/O_2$=1,21 D = 4cm, t = 2h, RMS=2.75 nm

Increasing the deposition time or the substrate temperature have the effect of increasing roughness and morphology change, respectively.

For titanium oxide there is a transition from the amorphous columnar appearance (substrate at room temperature, RMS = 0.11 nm) to a nanostructured with oriented crystallites (substrate heated at 500 $^0$C, RMS = 4.5 nm). The surface morphology of thin films of silicon oxide highlights a porous structure with amorphous clusters (RMS = 0.91 nm) which significantly increases as the deposition time (RMS = 2.75 nm) and the substrate temperature increases. The results are in good agreement with those of the X-ray diffraction.

### 3.3.1.3. Investigation of morphology and composition of the interferential system deposited on textile substrate

The $Ag/TiO_2/SiO_2/TiO_2/SiO_2/Ag$ multilayer system supported on cotton fabric was investigated using scanning electron microscopy (VEGA II LSHEDX - QUANTAX QX2).

SEM images highlight a uniform distribution of elements on the fabric surface. From the EDX spectrum were determined the concentrations of the main elements from the multilayer systems (Fig.3.24) and it was found that they are comparable to the

designed values obtained by choosing certain thickness of thin films.

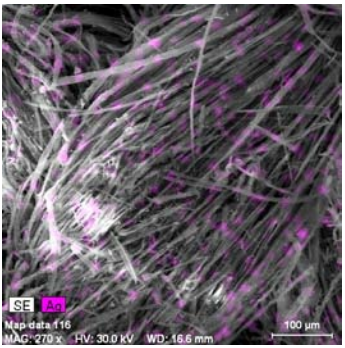


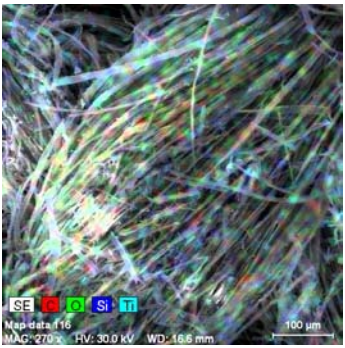


| C%at | Ti%at | Si%at | Ag%at | O%at |
|---|---|---|---|---|
| 14.87 | 0.49 | 2.69 | 0.08 | 82.19 |

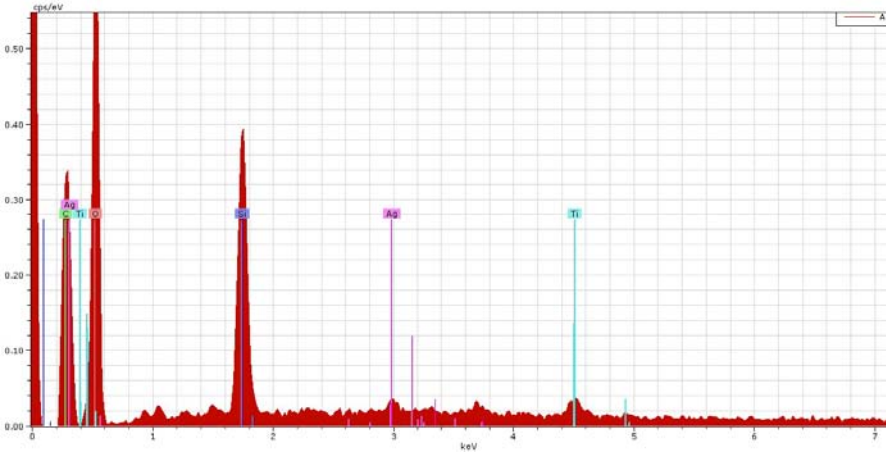


Fig.3.24. SEM analysis of the multilayer structure deposited on the fabric substrate: SEM images of the distribution of chemical elements, elemental chemical composition and EDX spectrum.

### 3.3.2. Analysis of the optical properties of the thin films and multilayer structures

#### 3.3.2.1. Transmittance and reflectance investigation of the metal thin films

In Figs. 3.25 and 3.26 are presented the transmittance and reflectance obtained for metal layers deposited on glass.

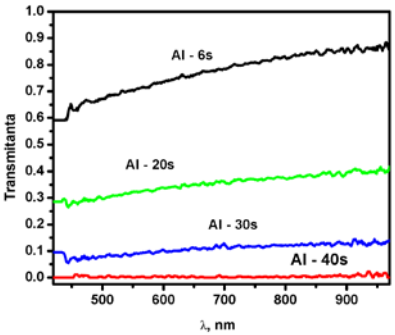


Fig.3.25. Deposition time dependence of the Al thin films (deposited on glass) transmittance.

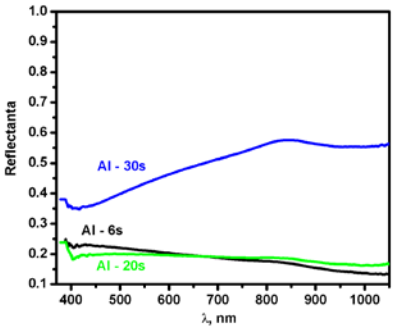


Fig.3.26. Thermal vacuum evaporation deposition time dependence of the Al thin films reflectance.

#### 3.3.2.2. Investigation of the multilayer thin films transmittance and reflectance

As can be seen from Fig. 3.27 b) and c), the $TiO_2$/Al/glass systems deposited on the $250^0$C heated substrate are transparent. Although they have the same thickness as the $TiO_2$/Al/glass systems, $SiO_2$/Al/glass systems deposited on the 100 $^0$C heated substrate have low visible light transparency, 30%, and become transparent at 1050 nm.

The optimal deposition conditions for the of $TiO_2$, $SiO_2$ oxide thin films were established and the influence of the substrate temperature and its thickness on the structure, roughness and optical properties was tracked.

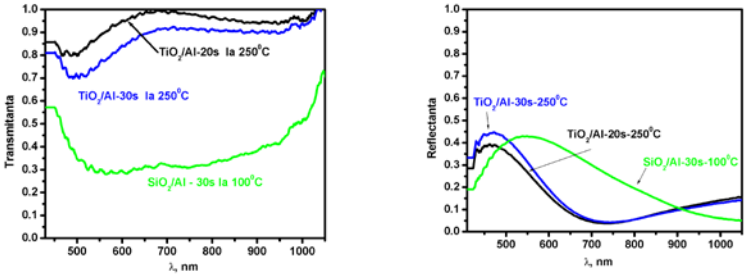


a) b)

Fig.3.27. The thin layer transmittance (a) and reflectance (b) dependence on the nature of the oxide (deposited on glass covered with a metal layer of aluminum) and on the time of deposition of the metallic layer, for different temperatures of substrate heating.

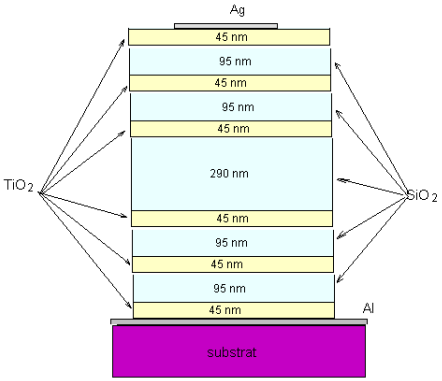


Fig.3.10. Multilayer structure designed for interferential filter.

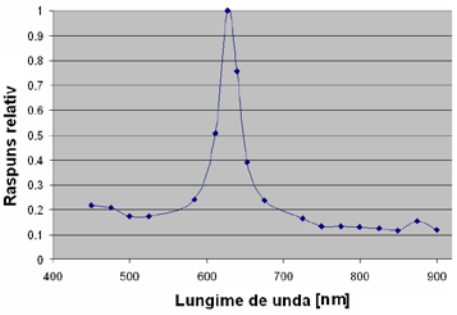


Fig. 3.33. The characteristic of the photo-detector with an integrated selective filter made according to IMT-Bucharest technology

# CHAPTER IV

# STUDY OF THE FUNCTIONAL THIN FILMS WITH POSSIBLE APPLICATIONS IN SPINTRONIC DEVICES AND SENSORS

## 4.1. Introduction

In order to obtain thin films of titanium oxide doped with manganese to achieve specific properties for certain applications, I chose two methods: ion implantation and magnetron sputter deposition. The study of the deposition conditions effect on the structure and properties of the resulted thin films was very important.

To obtain $La_{0,6}Pb_{0,4}MnO_3$ thin layers for applications in spintronic devices and sensors, powders of $La_{0,6}Pb_{0,4}MnO_3$ synthesized by the self-combustion method were used for the targets fabrication. Magnetic properties of thin films were investigated using electron spin resonance spectroscopy.

Conductive and transparent oxide of Ga-doped zinc oxide (GZO) has pointed out due to the high transparency and low price. In this study we aimed to obtain GZO thin films and investigate their functional properties for potential applications in transparent electronics and sensors.

## 4.2. Technological experiments for functional layers deposition

### 4.2.1. Deposition of $Mn_xTi1_{-x}O_2$ thin films by ion implantation

Mn-doped $TiO_2$ thin films were obtained by means of the ion implantation with doses of: 3% Mn: $8.53 \cdot 10^{15}$ $cm^{-2}$, 5% Mn: $1.42 \cdot 10^{16}$ $cm^{-2}$ şi 7% Mn: $1.99 \cdot 10^{16}$ $cm^{-2}$. Implantation was performed at the Technical University of Braunschweig, Germany

using a Varian extrion 200 DF 4 equipment. As targets (substrate) $TiO_2$ (rutile) single crystal wafers were used. Mn ions with a maximum energy of 200 keV were obtained by sublimation $MnI_2$.

### 4.2.2. Deposition of $Mn_xTi_{1-x}O_2$, $La_{0,6}Pb_{0,4}MnO_3$ and $Ga_{0,02}Zn_{0,98}O$ thin films by RF magnetron sputtering

In order to obtain semiconductor thin films with controllable optical and magnetic properties, titanium oxide targets with different atomic concentrations of Mn: 0.0 to 16.0% Mn were made by three processes:

1. Mechanical mixing of the oxides of titanium and manganese in a ball mill, $MnO_2/TiO_2$ ratio being calculated in order to have the desired content in atomic percent, followed by pressing into a pellet having a diameter of 40 mm and a thickness of 2 mm and heat treatment at 600 $^0$C for 1 h (Fig.4.2, Fig.4.3).
2. Make a slurry in isopropyl alcohol of the mixture of oxides carried out as in process 1, applying it on a 40 mm copper disc, in successive layers and drying with a hair dryer.
3. The obtaining nanostructured titanium oxide powder doped with Mn by a modified sol-gel method and perovskite powder ($La_{0,6}Pb_{0,4}O_3$) using the self-combustion method, respectively, and target achievement by one of the two methods presented above.

To achieve the targets for rf magnetron sputtering using the first method, a mold was designed and made. The mold was made of steel used for ISO 4957:1999 tools and has the following components (Fig. 4.2): guiding column, injection nozzle (40 mm in diameter), pressure plate, spring.

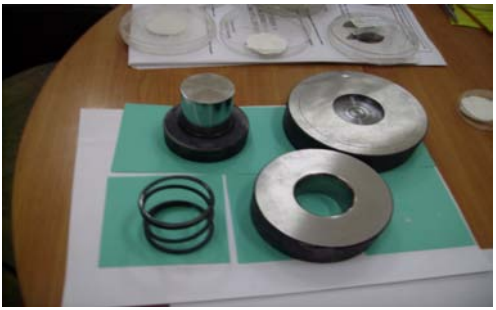

a)

b)

Fig.4.2. Forming mold for oxide targets: a) mold components b) target appearance obtained by pressing titanium oxide powder and heat treatment at $600^0$C.

In the procedure for the oxide targets preparation we can highlight the following steps: cleaning the mold, determining the chemical composition of the target, weighing necessary quantities of oxides, oxide powder mixture entering in the die space provided (photo), powder pressing using a hydraulic press and subjecting the target to heat treatment.

10% Mn

$La_{0,6}Pb_{0,4}O_3$

There have been attempts to deposit $TiO_2$ thin films doped with different concentrations of Mn. For deposition VUP 5M system was used. Different substrate-target distances (2-6 cm), different deposition times (30min-3h), rotary support with adjustable rotation speed and the substrate temperature maintained at room temperature were used. Thin films were deposited on glass substrates, quartz and $SiO_2$/Si. The layer thickness resulted from

the 3 hours deposition was measured by SEM and found to be de150 nm.

Following the deposit process, the thin films were subjected to heat treatment at 550 $^0$C for 1 h or 2 h and at 800 $^0$C for 1 h, respectively. Thin films were subjected to structural and compositional characterization.

For gallium-doped zinc oxide thin layers deposition, ZnO target doped with 2 wt.% $Ga_2O_3$, of 99.99%purity, commercially available, with a diameter of 40 mm and a thickness of 2 mm. As spraying gas, argon gas with a purity of 99.99% was used. The total pressure in the system was maintained at 3 mtorr throughout the deposit.

## 4.3. Investigation of the structure, morphology and chemical composition of the functional layers

### 4.3.1. Investigation of the structure and morphology of thin films obtained by ion implantation

The chemical composition and morphology of $Mn_xTi_{1-x}O_2$ thin films obtained by ion implantation were investigated using scanning electron microscopy (SEM, EDX) SCM Instrument JSM-5600, equipped with an X-ray energy dispersion analysis system. For structural analysis the X-ray diffraction (DRON 2 CoKα, λ = 0.178892 nm) was used. The morphology and surface roughness were investigated using atomic force microscopy (NT - MDT Solver Pro 7M).

EDX analysis of manganese ion implanted rutile single crystals revealed Mn contents of 3%, 5% and 7% (atomic percent). The chemical formulas of the formed thin layers on implanted surface can be expressed as: $Mn_{0,03}Ti_{0,97}O_2$; $Mn_{0,05}Ti_{0,97}O_2$ and $Mn_{0,07}Ti_{0,93}O_2$, according to the simulation performed for implantation (Fig.4.5).

XRD patterns of the samples implanted with Mn and those of the samples annealed at 600$^0$C highlights the intense XRD

peaks of rutile (R) and some low intensity peaks attributed to anatase phase (A) and brookit phase (B). All diffractograms were recorded in the same conditions.

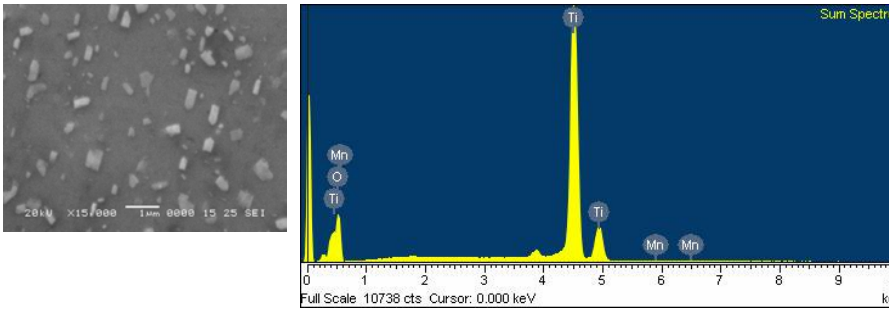


Fig.4.5. SEM and EDX analysis of the $Mn_{0,05}Ti_{0,97}O_2$ sample heat treated at $600^0$C

XRD patterns of samples implanted with Mn and not subject to the thermal treatment highlights the partial destruction of the crystal surface (Fig.4.6) [19].

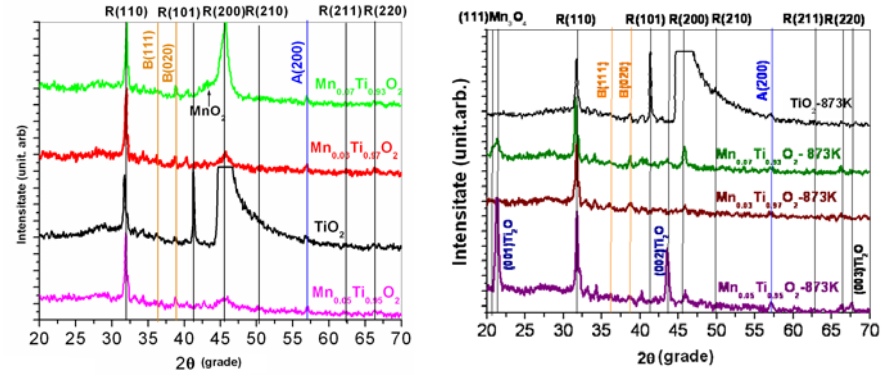


a) b)

Fig.4.6. XRD patterns of the a) ion implanted and b) heat treated at $600^0$C for 1h $Mn_xTi_{1-x}O_2$ samples

In samples with Mn concentrations of 7%, the appearance of XRD peaks attributable to $MnO_2$ antiferromagnetic phase and $Mn_2O_3$ ferromagnetic phase is observed.

Unit cell parameters were determined using the XLAT-Cell Constant Rafinement program and thin films crystallite size was determined using Scherrer formula. The results are listed in Table 4.1, together with observed crystalline phases.

The samples surfaces show a dense microstructure with nanosized crystallites with tetragonal or hexagonal symmetry.

Nanoparticle size determined from 3X3 μm AFM images (Fig.4.6) are in agreement with those determined from the diffraction pattern. For all studied samples, surface roughness is higher for samples heat treated, the RMS being below 9 nm (Table 4.1).

Tabelul 4.1**.** The unit cell parameters (a, c), the crystallite size (D) and the phase of the rutile samples (100) implanted with ions of Mn

| Proba | a nm | c nm | c/a | D nm | Faze cristaline |
|---|---|---|---|---|---|
| $TiO_2$ | 0.427 | 0.3039 | 0.6568 | | Rutil |
| $TiO_2$-873K | 0.4625 | 0.3025 | 0.6540 | | Rutil |
| $Mn_{0.03}Ti_{0.97}O_2$ | 0.4604 | 0.2973 | 0.6458 | 8.29 | Rutil |
| $Mn_{0.03}Ti_{0.97}O_2$ -873K | 0.4600 | 0.2973 | 0.6464 | 23.34 | Rutil |
| $Mn_{0.05}Ti_{0.95}O_2$ | 0.4658 | 0.2994 | 0.6427 | 4.79 | Rutil |
| $Mn_{0.05}Ti_{0.95}O_2$-873K | 0.4623<br>0.3002 | 0.3008<br>0..4835 | 0.6506<br>1.611 | 26.37<br>20.97 | Rutil<br>$Ti_2O$ |
| $Mn_{0.03}Ti_{0.97}O_2$ | 0.4529 | 0.3124 | 0.6761 | 8.40 | Rutil |
| $Mn_{0.07}Ti_{0.93}O_2$ -873K | 0.4605<br>0.3002 | 0.3090<br>0.4840 | 0.6709<br>1.612 | 31.32<br>5.77 | Rutil<br>$Ti_2O$ |

In order to elucidate the surface microstructure, investigations were carried out by scanning electron microscopy. In Fig.4.4. a nanostructured surface aspect is highlighted for the $Mn_{0,05}Ti_{0,97}O_2$ – 873K sample. The manganese map obtained for this image revealed that a large part of the surface nanocrystallites

have low Mn contents or not at all. This observation supports the Mn migration within the substrate idea.

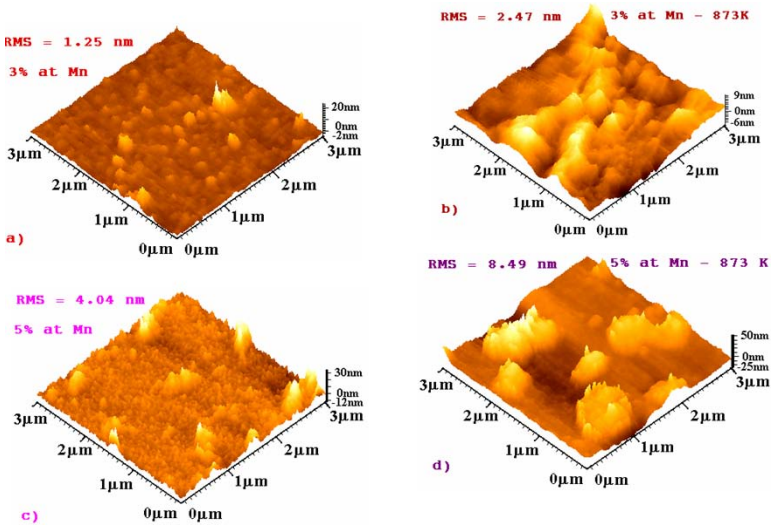


Fig.4.7. 3x3μm 3D AFM images of 3% Mn (a and b) and 5 % Mn (c and d) before and after heat treatment at 600ºC samples.

### 4.3.2. Investigation of the structure, chemical composition and morphology of thin films obtained by sputtering

#### 4.3.2.1. The structure of $Mn_xTi_{1-x}O_2$ thin films deposited using oxide targets

Thin films deposited on glass substrates, quartz and $SiO_2$/Si were structural and compositional analyzed immediately after the deposition process. The XRD patterns of all samples revealed amorphous structure whatever the substrate.

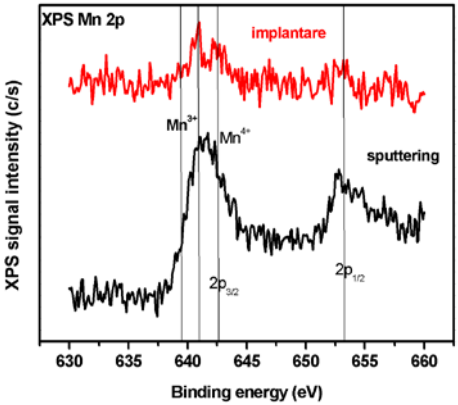


Fig.4.10. Mn2p XPS spectra of $Ti_{0,95}Mn_{0,05}O_2$ thin films obtained by ion implantation and magnetron sputtering, heat treated.

XPS analysis of the Mn 2p, Ti 2p and O1s elements revealed a chemical composition similar to the targets, especially for samples deposited from targets made of $Mn_xTi_{1-x}O_2$ compounds obtained by sol-gel synthesis.

### 4.3.2.2. The structure of $Mn_xTi_{1-x}O_2$ thin films deposited using co-deposit method

XRD patterns recorded for the initial samples and for those heat treated at 400 $^0$C for 30 minutes, revealed the nanocrystalline thin films. Analysis of XPS spectra for the Ti 2p, Mn 2p and O1s elements revealed a XPS peak dependence of the RF power, an increase of peak intensity with increase in Mn content. AFM study revealed that there is a linear dependence of the thin films roughness of the rf power.

### 4.3.3. Structural and morphological analysis of the LPMO thin films deposited by sputtering (RF sputtering)

In Figs. 4.16 and 4.17 are presented the XRD patterns corresponding to the LPMO thin films obtained by cathodic spraying method (RF sputtering) using perovskite $La_{0,6}Pb_{0,4}MnO_3$ as target material and quartz or alumina as substrate.

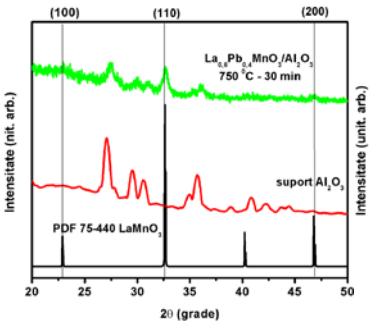


Fig. 4.16. XRD patterns of the substrate (alumina) and LPMO thin film deposited on it.

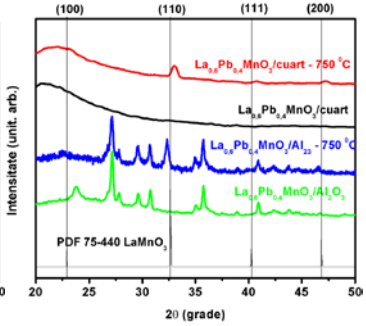


Fig. 4.17. XRD patterns of the LPMO thin films deposited on alumina or quartz substrates before and after heat treatment.

XRD patterns obtained for the heat treated thin films in air at 750 °C for 30 min. show characteristic XRD peaks of lanthanum manganite, $LaMnO_3$. The layers obtained are crystalline cubic symmetry (Pm3m space group) and do not present foreign phases. This can be explained by the composition of the target reflected in the composition of the thin layer due to optimum deposition parameters (deposition time of 120 min, distance target-substrate of 2 cm, rf power of 75 W, gas ratio $O_2/(O_2+Ar)=1/(1+9)$) and subsequent heat treatment.

### 4.3.4. Structural, morphological and compositional analysis of the thin layers of zinc oxide doped with gallium

Based on obtained data from diffraction patterns, unit cell parameter values, c, and the average size of crystallites were determined (Tab.4.2).

**Tabelul 4.2.** Structural information obtained from XRD and AFM for zinc oxide doped with gallium

| **Sample** | **$T_s$ ($^oC$)** | **(hkl)** | **$d_{hkl}$ (nm)** | **D (nm)** | c **(nm)** | $\sigma_{film}$ (GPa) | **δx10$^{-8}$ (nm$^{-2}$)** | **RMS (nm)** |
|---|---|---|---|---|---|---|---|---|
| **Ga: ZnO** | 200 | 002 | 0,261 | 19 | 0.521 | 0,86 | 25 | 21,47 |

Ts - substrate temperature; **(**hkl) - Miller indices; $d_{hkl}$ - interplanar distance; D - the average size of crystallites; c - crystalline network parameter; σ – internal tension; δ - dislocation density, RMS - RMS surface roughness.

No XRD peaks belonging to other crystalline phases were presented and this can be explained by the fact that Ga ions substitute Zn ions in a crystalline zinc oxide network.

XPS spectra were recorded using a XPS SPECS PHOIBOS 150 MCD equipment (Al Kα source, 1486.6 eV).

The binding energy of Zn $2p_{3/2}$ at 1021.29 eV confirms the status of $Zn^{2+}$ in an oxygen deficient ZnO matrix, this value being slightly smaller than the binding energies of $Zn^{2+}$ in ZnO. Ga 2p XPS spectra clearly show the presence of XPS peaks corresponding to Ga $2p_{3/2}$ and Ga $2p_{1/2}$ centered at 1116.93 eV or 1143.75 eV. The results were in good agreement with those reported in the literature, confirming that the $Ga^{3+}$ ions substitute the $Zn^{2+}$ atoms in the crystal lattice of the ZnO.

## 4.4. Functional characterization of thin films deposited by magnetron sputtering method

### 4.4.1. Experimental studies of gas sensitivity

To measure the sensitivity of the materials based on thin films of titanium oxide doped with Mn, zinc oxide doped with gallium and La-Pb manganese, the samples were mounted on a heater and placed in a glass chamber capable of controlling different concentrations gas in the temperature range between $100^{o}C \div 400^{o}C$.

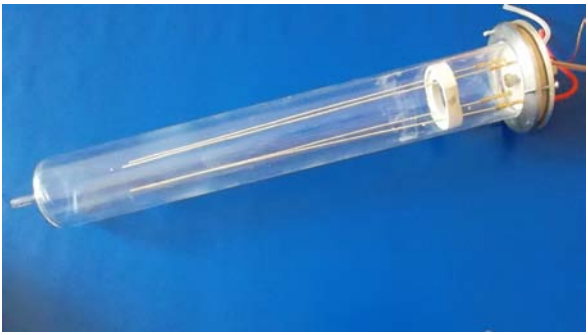

Fig.4.21. Quartz enclosure for gas sensitivity measurements

The temperature at which the sensitivity of the doped zinc oxide layer with gallium/glass was determined was varied in the range of 373K - 673K and gas. The gas concentration of 800 ppm was used as it was observed that for this value of the concentration of the oxide layer gallium-doped zinc/glass the highest sensitivity was obtained.

For such an investigation a quartz chamber was made, which can be inserted into a tube furnace, with the possibility to connect to the gas tube (Fig.4.21).

It is noted that the higher the temperature the sensitivity value of the gas increases and reaches a maximum at a temperature of 633 K, after which the sensitivity begins to decrease at higher temperatures.

The turnaround time was 50 sec. for 800 ppm ethanol at an operating temperature of 633K. The optimum operating temperature for the studied sample was determined to be 633 K for all gases studied.

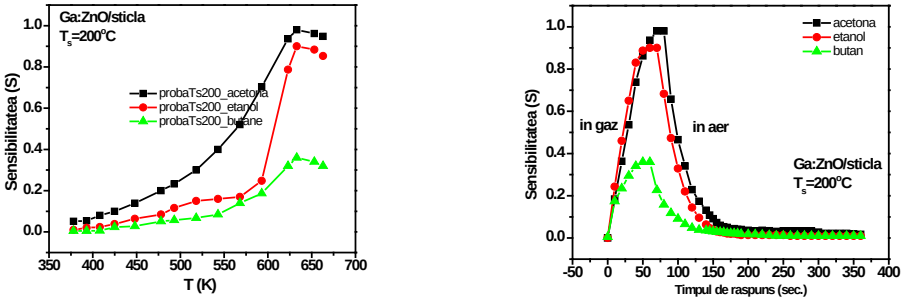


Fig .4.22 Sensitivity dependencies of the temperature (a) and of the response time for the gallium-doped zinc oxide/ lass (b).

Analysis of the gas sensitivity of titanium oxide doped with Mn thin films highlighted the selectivity of these compounds for acetone at concentrations of 2000 ppm.

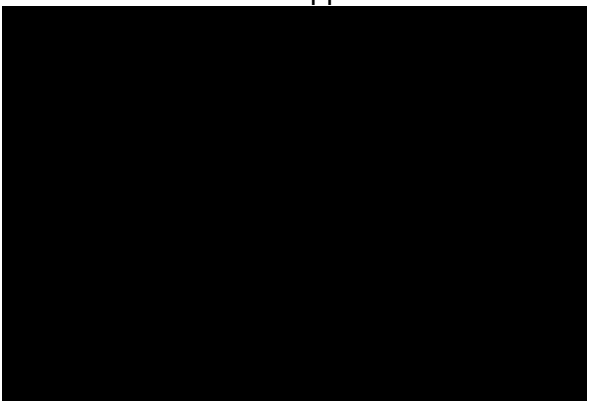

Fig. 4.15. Studied gas sensitivity characteristics depending on operating temperatures for thin films deposited using $La_{0,6}Pb_{0,4}MnO_3$.

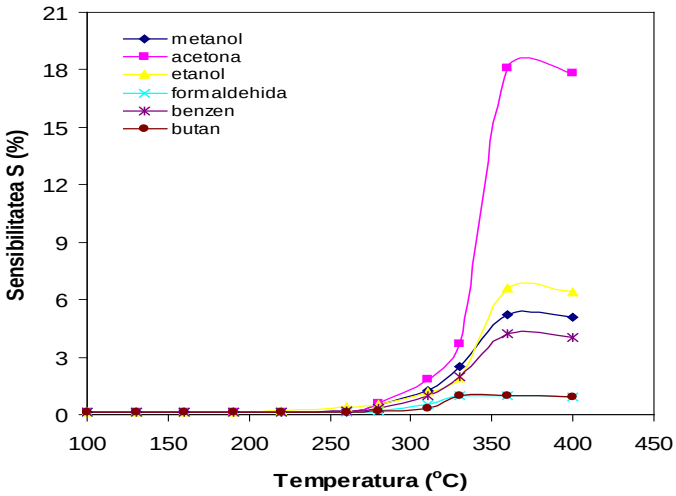


Fig. 4.16. Studied gas sensitivity characteristics depending on operating temperatures for $TiO_2$ – 10%Mn.

Tabelul 4.3 Operating temperature and response times for the gallium-doped zinc oxide/Glass

| Test gas | Response time (s)<br>Zinc oxide doped with gallium | Operating<br>Temperature (K) |
|---|---|---|
| Ethanol | 50 | 633 |
| Acetone | 60 | 633 |
| Butane | 53 | 633 |

For perovskites, the maximum sensitivity was highlighted for methanol under the same conditions

### 4.4.2. The study of magnetic properties using electronic spin resonance

### 4.4.2.1. The study of magnetic properties of $Ti_{1-x}Mn_xO_2$ thin films

As can be seen in Fig.4.26, after ion implantation, the samples show broad signals at values of g=2, $\Delta B$ = 100 mT, the most intense signal belonging to $Ti_{0,97}Mn_{0,3}O_2$ sample. Over this signal RES signals of $Mn^{2+}$ and of some defects in the structure are superimposed. The broad signal disappears after heat treatment and the narrow lines attributed to structural defects appear more intense.

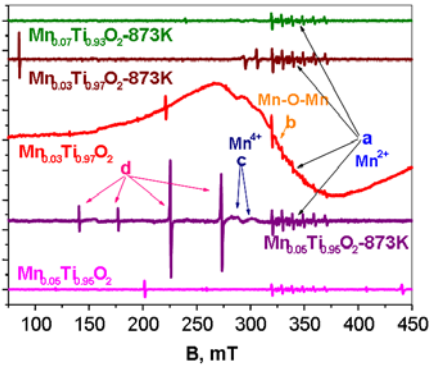


Fig.4.26. RES spectra of thin films obtained by ion implantation, before and after heat treatment

The broad signal disappearance indicate the migration of manganese ions from the inside surface of titanium oxide substrate to form new species that increase RES signals attributed to structure defects in the un-implanted area. The results are in good agreement with the results obtained by X-ray diffraction.

RES spectra of thin films deposited by sputtering highlights isolated $Mn^{4+}$ species and broad signals typical to the exchange interaction (Fig. 4.27, Fig.4.28). RES signals present an angular dependence, indicating a preferential

orientation of the magnetic moments, namely the existence of magnetic anisotropy.

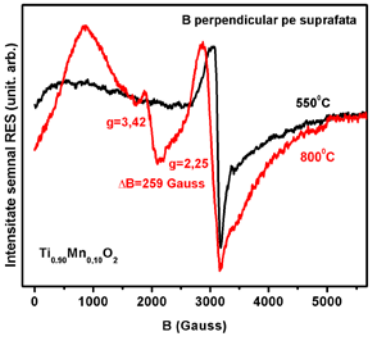


Fig.4.27. RES spectra of $Ti_{0,90}Mn_{0,10}O$ thin films, heat treated at 10°orientation of the magnetic field perpendicular to the surface layer.

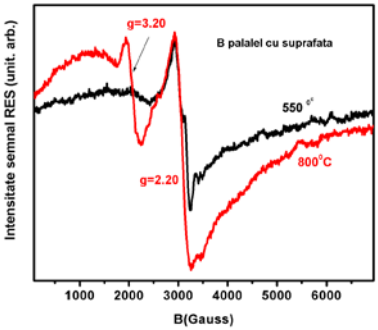


Fig.4.28. RES spectra of $Ti_{0,90}Mn_{0,10}O$ thin films, at 10 ° orientation of the magnetic field parallel to the surface layer.

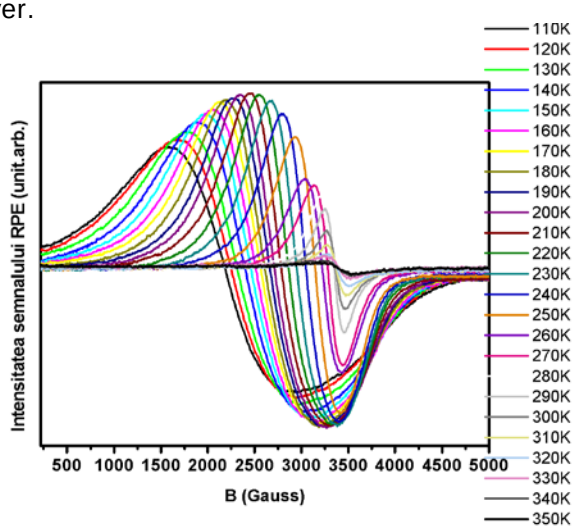


Fig.4.29. RES spectra of thin films $La_{0,6}Pb_{0,4}MnO_3$ as a function of temperature

By means of the heat treatment the magnetic properties of the layers are improved as a result of eliminating tensions and rearrangement of atoms in the network.

For thin layers of Pb doped lanthanum manganese is found that, starting from the temperature of 300K to lower values, RES signal moves to lower values of the magnetic field and increases in intensity and width up to 200 K, after which the intensity begin to fall Fig.4.29). Towards elevated temperatures, the signal moves to higher magnetic fields, slightly increasing the intensity and breadth. RES signal occurs due to the presence of $Mn^{4+}$isolated ions and of $Mn^{3+}$- $Mn^{4+}$ Zener pairs. This dual exchange involves a series of events including the metal-semiconductor phase transition from paramagnetic to ferromagnetic, respectively.

## Conclusions

In this thesis the main original results obtained from the structural, morphological and compositional characterization of the thin films and multilayer structures are presented. Also original results obtained from the analysis of the optical, magnetic and as sensor properties for use in various functional applications are shown. Thus, the thesis studied four types of systems, namely thin films and multilayer structures based on $TiO_2$ and $SiO_2$ obtained by rf sputtering, thin layers of titanium oxide doped with Mn, thin layers of lanthanum manganite doped with Pb and zinc oxide thin film doped with Ga. The following original contributions can be highlighted:

1. Metallic materials and oxide materials suitable for making multi-layer structures with selective spectral properties were selected.

2. Improvements on VUP-5M deposit facility were made by designing the rotating system of the samples and masks, and by adaptation the heating system of the substrate, in order to achieve rotation and simultaneous heating of the substrates.

3. The deposition conditions of the metal layers have been investigated, the optimal conditions for deposition of $TiO_2$, $SiO_2$ oxide thin films were established and the influence of substrate temperature on the structure and its thickness, roughness and optical properties were followed.

4. Different multilayer systems were analyzed, which currently has an optimal flow sheet. The considered systems operate as reflective or antireflective systems. The integration of multilayer system, consisting $TiO_2$, $SiO_2$ 11 layers, in front of a photo-detector has led to a visible band pass filter.

5. Thin layers of titanium oxide doped with Mn in concentrations selected to confer some ferromagnetic properties at room temperature or as sensor were made.

6. Three methods of deposition were used: ion implantation, sputtering and co-deposition of two metal targets. We have found that through ion implantation, a local destruction of the crystal lattice takes place, which may be adjusted by heat treatment. The most ferromagnetic layers at room temperature were found to be those with 5% Mn.

7. The studies realized on sputter deposited thin layers revealed that the magnetic properties of the samples are much higher for the sample with 10% Mn, especially after a heat treatment performed at $800^0$C.

8. It has been shown that the use of co-deposition method, the Mn content and the roughness of the the layers depend on the power applied to the Mn target, the slope of the linear dependency becoming greater for powers greater than 35W.

9. The studies performed on thin layers deposited by RF magnetron sputtering from targets made by us of powders synthesized by self-combustion method show that they have the necessary qualities for their application in spintronic devices, namely the sensor.

10. The sensor properties approach of the zinc oxide thin films doped with 2% Ga has proven to be successful, hsving a high sensitivity and selectivity for acetone.

11. The experimental results lead to the conclusion that we have chosen the correct study materials and the dopant concentrations that elicited thin and multilayer structures, which can be can be used as active elements in transparent electronics and spintronics sensors.

**KEYWORDS:** oxide thin films, multilayer structures, ion implantation, sputtering, functional properties

## Selected references

[1] D. Bhattacharyya, N.K. Sahoo, S. Thakur, N.C. Das, Vacuum 60 (2001) 419
[2] H. Selhofer and R. Müller, Thin Solid Films 351 (1999) 180
[3] C. Garapon, J. Mugnier, G. Panczer, B. Jacquier, C. Champeaux, P. Marchet and A. Catherinot, Appl. Surf. Science 96-98 (1996) 836.
[4] M.F. Ouellette, R.V. Lang, K.L. Yan, R.W. Bertram, R.S. Owies and D. Vincent, J. Vac. Sci. Technol. A. 9 (1991) 1188
[5] C. Rickers and M. Vergöhl, Thin Solid Films, 442 (2003) 145
[6] F. Hamelmann, G. Haindl, J. Schmalhorst, A. Aschentrup, E. Majkova, U. leineberg, U. Heinzmann, A. Klipp, P. Jutzi, A. Anopchenko, M. Jergel, S. Luby, Thin Solid Films, 358 (2000) 90
[7] X. Wang, H. Sumoto, Y. Someno, T. Hirai, Appl. Phys. Lett. 72 (1998) 3264.
[8] J. Szczyrbowski, G. Brauer, G. Teschner, A. Zmelty, Journal of Non Crystalline Solids. 218 (1997) 25.
[9] M. Alvisi, L. Mirenghi, L. Tapfer, A. Rizzo, M.C. Ferrara, S. Scaglione, L. Vasanelli, Applied Surface Science, 157(1-2) (2000) 52
[10] L. Martinu, D. Poitras, Journal of Vacuum Science & Technology A Vacuum, Surfaces, and Films, 18 (2000) 2619.
[11] J. Boudaden, R. S-C. Ho, P. Oelhafen, A. Schüler, C. Roecker and J. - L. Scartezzini, Solar Energy Materials and Solar Cells, 84 (2004) 225.

[12] A. Schüler, C. Roecker, J. - L. Scartezzini, J. Boudaden and P. Oelhafen, Solar Energy Materials and Solar Cells, 84 (2004) 241
[13] G. Minas, R. F. Wolffenbuttel, J. H. Correia, J. Optics A:Pure Applied Optics, 8 (2006) 272-278.
[14] F. Iacomi, N. Apetroaei, G. Calin, **Gh. Zodieriu**, M.M. Cazacu, C. Scarlat, V. Goian, D. Menzel, I. Jursic, J. Schoenes, Thin Solid Films 515 (2007) 6402.
[15] N.S. Gluck, H. Sankur, J. Heuer, J. DeNatale and W.J. Gunning, J. Appl. Phys. 69 (1999) 3037
[16] A. Tabata, N. Matsuno, Y. Suzuoki and T. Mizutani, Thin Solid Films 289 (1996) 84
[17] Optical properties of coating materials from Sopra S.A., website: http://www.sopra-sa.com, (2006).
[18] W. Wong, H. Masumoto, Y. Someno, L. Chen and T. Hirai, J. Vac. Sci. Technol. B. 18 (2000) 933
[19] J. K. Dewhurst and J. E. Lowther, Physical Review B 54 (1996), R3673. J. Haines and J. N. Léger, Physica B 192 (1993), 233

## List of publications

**Papers published in ISI journals**

1. F. Iacomi, N. Apetroaei, G. Calin, **Gh. Zodieriu**, M.M. Cazacu, C. Scarlat, V. Goian, D. Menzel, I. Jursic, J. Schoenes, **Structure and surface morphology of Mn-implanted TiO2, Thin Solid Films**, vol. 515, pp. 6402-6406, iunie 2007. (factor de impact = 1,693) (AIS= 0,642).
2. A. Yildiz, M. Irimia, M. Dobromir, D. Timpu**, G. Zodieriu,** F. Iacomi, **Studies on electron transport in gallium-doped zinc oxide thin films,** J. Appl. Phys., trimisa spre publicare.
3. M. Irimia, A. P. Rambu, **G. Zodieru**, I.I. Leonte, M. Purica, F. Iacomi, **„Ga doped ZnO thin films deposited by RF magnetron sputtering – preparation and properties”**, Proc. of IEEE International Semiconductor Conference CAS

2011, Sinaia, Romania, 17-19 Oct. 2011, pp. 287-290 (factor de impact = 0) (AIS= 0).

**Participations to international conferences: 7**
**Participations to national conferences:1**